Prostaglandin E$_2$–Dependent Blockade of Actomyosin and Stress Fibre Formation Is Mediated Through S1379 Phosphorylation of ROCK2

Casimiro Gerarduzzi,[1,3]* QingWen He,[2] John Antoniou,[4] and John A. Di Battista[2,3]

[1]*Department of Genetics and Complex Diseases, Harvard School of Public Health, Boston, Massachusetts*

[2]*Department of Medicine, McGill University, Montreal, Quebec, Canada*

[3]*Department of Experimental Medicine, McGill University, Montreal, Quebec, Canada*

[4]*Department of Orthopaedic Surgery, Jewish General Hospital, Montreal, Quebec, Canada*

ABSTRACT

Prostaglandin E$_2$ is a pleiotropic bioactive lipid that controls cytoskeletal alterations, although the precise G-protein coupled EP receptor signalling mechanisms remain ill defined. We adopted a phosphoproteomic approach to characterize post-receptor downstream signalling substrates using antibodies that selectively recognize and immunoprecipitate phosphorylated substrates of a number of kinases. Using human synovial fibroblasts in monolayer cell culture, PGE$_2$ induced rapid and sustained changes in cellular morphology and reduction in cytoplasmic volume that were associated with disassembly of the phalloidin-stained stress fibres as judged by light and confocal microscopy. Furthermore, PGE$_2$ induced a rapid dephosphorylation of myosin light chain II (MLC) at S19 under basal or cytokine-induced conditions that was linked to an activation of myosin light chain phosphatase. The use of specific synthetic EP agonists suggested that the response was mediated by EP2 receptors, as other EP agonists did not manifest the same effect on MLC phosphorylation. In addition, PGE$_2$ induced sustained Y118 dephosphorylation of phospho-paxillin and loss of focal adhesions as observed by confocal microscopy and Western analysis. Phosphoproteomic analysis of PGE$_2$/GPCR/PKA phosphosubstrates identified a unique, non-redundant, phosphorylated (>30-fold) site on rho-associated coiled coil-containing kinase 2 (ROCK2) at S1379. Analysis of ROCK2 mutant behaviour (e.g. S1379A) in overexpression studies revealed that PGE$_2$-dependent phosphorylation of ROCK2 resulted in the inhibition of the kinase, since induced MLC phosphorylation was no longer blocked by PGE$_2$ nor could PGE$_2$ induce disassembly of stress fibres. Thus, PGE$_2$-dependent blockade of actomyosin fibre formation, characteristic of myofibroblasts, may be mediated through specific ROCK2 S1379 phosphorylation. J. Cell. Biochem. 115: 1516–1527, 2014. © 2014 Wiley Periodicals, Inc.

KEY WORDS: FIBROBLASTS; MYOFIBROBLASTS; FIBROSIS; PROSTAGLANDIN E$_2$ (PGE$_2$); ROCK2; STRESS FIBRES; MYOSIN LIGHT CHAIN

Fibroblast–myofibroblast transitions (FMTs) are essential for normal wound healing in that fibroblasts activate and differentiate into myofibroblasts, migrate to the site of injury and remodel the pericellular and extracellular matrix (ECM) [Desmoulière et al., 2003; Hinz, 2010]. This remodeling occurs in part through deposition of type I collagen and other matrix/structural proteins (laminins, elastins, tenascins), and through

contraction of the wound via increased α-smooth muscle actin (α-SMA) expression and activity [Hinz et al., 2001; Desmoulière et al., 2003; Guarino et al., 2009]. Once tissue is repaired, myofibroblasts are then primed to undergo apoptosis [Desmoulière et al., 2003]. In fact, there is evidence that failure of myofibroblasts to apoptose, likely the result of the persistent extracellular matrix (EMT) tension, accounts for the continuous synthesis of matrix

1516

products and fibrous plaques formations, limiting normal tissue repair and mechanical integrity [Hinz, 2010]. Similarly, epithelial–mesenchymal transitions (EMT) participate in tissue repair but also pathological processes such as fibrosis, tumour invasiveness and metastasis [Guarino et al., 2009]. Indeed, like myofibroblasts, the mesenchymal cell phenotype can be characterized by changes in gene expression, and by enhanced migratory capacity, invasiveness and elevated resistance to apoptosis [Horowitz and Thannickal, 2006; Guarino et al., 2009]. Pulmonary and liver fibrosis, post-myocardial infarction lesions, tumour invasiveness/cancer, synovial tissue fibrosis in rheumatoid arthritis, and skin diseases like systemic scleroderma are life-threatening pathologies associated with aberrant FMT/EMT [Desmoulière et al., 2003; Horowitz and Thannickal, 2006; Steenvoorden et al., 2006; Akhmetshina et al., 2008; Butcher et al., 2009].

The regulation of myofibroblast differentiation is a critical control point in normal and pathological tissue repair responses. TGF-β and ECM tension are the pivotal cues required for transiting into the myofibroblast phenotype [Tomasek et al., 2002]. Although both factors are necessary, higher levels of mechanical stiffness within the ECM brings about the later fully differentiated myofibroblast [Hinz, 2007]. Myofibroblasts interpret and respond to these external forces through counteracting tensional forces generated by cytoskeletal remodelling and actomyosin contraction. As myofibroblasts build up the ECM tension, a positive feedback loop is achieved and sustains this repair phenotype until the original structure of the ECM is reconstituted and again takes over the mechanical load.

The prominent signalling pathway that supports myofibroblastic contraction is the rho-associated coiled coil-containing kinase 2 (ROCK2)-dependent pathway [Tomasek et al., 2006; Akhmetshina et al., 2008]. In this connection, the protein encoded by the ROCK2 gene is a serine/threonine kinase that regulates cytokinesis, smooth muscle contraction, as well as the formation of actin stress fibres and focal adhesions (FA) [Ishizaki et al., 1996]. The actin cytoskeleton adheres to surrounding extracellular matrix (ECM) through FAs that serve as anchor points for stress fibres. Mechanical tension generated from the ECM signal the FA complex to activate the RhoA/ROCK2/Myosin II pathway in order to generate contraction from stress fibre formation for structural reinforcement [Besser and Schwarz, 2007; Vicente-Manzanares et al., 2009]. Activated ROCK2 can increase myosin-induced contractions directly by phospho-activating the myosin light chain (MLC) at Ser19 and indirectly by phospho-inhibiting myosin phosphatase (MYPT) at Thr853, which is the phosphatase responsible for dephosphorylating and inactivating myosin. Furthermore, modulating the phosphorylation status of the myosin II light chain by the RhoA effector ROCK2 directly affects stress fibre formation and concomitant paxillin phosphorylation (FA maturation) [Amano et al., 1996; Ramachandran et al., 2011].

RhoA, a small GTPase and Ras homolog, is phosphorylated and its activity moderated by the activation of protein kinase A (PKA), although the precise mechanisms, particularly with regard to the role of other tandem activated kinases, are ill defined [Dong et al., 1998; Howe, 2004]. Among the more prominent ligands for PKA regulation involves PGE$_2$, which signals through its G-protein coupled receptors (GPCRs) EP1 to EP4 [Funk, 2001]. The PGE$_2$/EP2/EP4 system has been shown to impact on fibroblast cytoskeletal rearrangements in part through inhibition of alpha-smooth muscle actin gene expression [Kolodsick et al., 2003; Thomas et al., 2007]. In order to characterize post-PGE$_2$-receptor downstream signalling substrates involved in cytoskeletal rearrangements, we used antibodies that selectively recognize (and immunoprecipitate) phosphorylated substrates of PKA with high stringency. The substrate motif used in this study recognizes phosphorylated serine/threonine in the context of arginine or lysine residues at the -2 and/or -3 position [(K/R)(K/R) X(s/t)]. After generation and enrichment of phosphopeptides, LC-MS-MS (LTQ-Obitrap-CID) was performed in tandem with quantitation and bioinformatical analysis (Phospho-Scan^{TM}). We identified some 150 PGE$_2$-dependent non-redundant phosphoproteins, many of which are associated with cytoskeletal regulation and organization. Here we report a unique, PGE$_2$-induced, functional inhibitory phosphoS1379 site on ROCK2 that mutational analysis confirms is critical to the activity of the enzyme in terms of myosin light chain II and paxillin phosphorylation, hence controlling the formation of stress fibres and FA in FMT.

EXPERIMENTAL PROCEDURES

CHEMICALS

Sodium fluoride, leupeptin, aprotinin, pepstatin, phenylmethylsulphonylflouride (PMSF), actinomycin D, dithiothreitol (DTT), sodium orthovanadate, DAPI, phalloidin, Y27632, forskolin, H89, KT-5720, Ro 20-1734, 8cPT-2Me-cAMP, transforming growth factor beta (TGF-β), lysophosphatidic acid (LPA), ATP and bovine serum albumin (BSA) were products of Sigma-Aldrich Canada (Oakville, Ontario, Canada). Prostaglandin E$_2$, butaprost, L-161982, a specific EP4 antagonist, and sulprostone were products of Cayman Chemical (Ann Arbor, MI) while L-902688, a specific EP4 agonist was a gift from Merck Frosst Canada (Pointe-Claire, Quebec).

Sodium dodecyl sulphate (SDS), acrylamide, bis-acrylamide, ammonium persulphate, and Bio-Rad protein reagent originated from Bio-Rad Laboratories Canada (Mississauga, Ontario, Canada). Tris-base, EDTA, MgCl$_2$, NaCl, CaCl$_2$, chloroform, dimethylsulphoxide (DMSO), anhydrous ethanol (95%), methanol (99%), formaldehyde and formamide were obtained from Fisher Scientific (Nepean, Ontario, Canada). Dulbecco's modified Eagle's medium (DMEM, Gibco), phosphate-free DMEM, Trizol reagent, heat inactivated foetal bovine serum (FBS), an antibiotic mixture [10,000 units of penicillin (base), 10,000 μg of streptomycin (base)], phosphate-buffered saline (PBS), and tetramethylethylenediamine (TEMED) were products of Invitrogen^{TM} (Burlington, Ontario, Canada).

SPECIMEN SELECTION AND CELL CULTURE

Synovial lining cells (human synovial fibroblasts, HSF) were isolated from synovial membranes (synovia) obtained at necropsy from donors with no history of arthritic disease (mean age 30 ± 27). Additional experiments were conducted (where indicated) with HSF specimens obtained from osteoarthritic (OA) and rheumatoid arthritic (RA) patients undergoing arthroplasty who were diagnosed based on the criteria developed by the American College of Rheumatology Diagnostic Subcommittee for OA/RA (mean age

67 ± 19) [Altman et al., 1986; Hochberg et al., 1992]. Human synovial fibroblasts were released by sequential enzymatic digestion with 1 mg/ml pronase (Boehringer Mannheim, Laval, Quebec, Canada) for 1 h, followed by 6 h with 2 mg/ml collagenase (type IA, Sigma-Aldrich) at 37°C in DMEM supplemented with 10% heat inactivated FBS, 100 units/ml penicillin and 100 µg/ml streptomycin. Released HSF were incubated for 1 h at 37°C in tissue culture flasks (Primaria #3824, Falcon, Lincoln Park, NJ), allowing the adherence of non-fibroblastic cells possibly present in the synovial preparation, particularly from OA and RA synovia. In addition, flow cytometric analysis (Epic II, Coulter, Miami, FL), using the anti-CD14 (fluorescein isothiocyanate, FITC) antibody, was conducted to confirm that no monocytes/macrophages were present in the synovial fibroblast preparation [Faour et al., 2005; Zhai et al., 2010]. The HSFs were CD45 negative and expressed no epithelial (e.g. EpiCAM) or endothelial markers but produce large amounts of hyaluronan and express high levels of hyaluronan synthase 2, VCAM-1, fibroblast-specific protein (FSP-1, S-100), prolyl-4-hydroylase and collagen type I a1 chain [Strutz et al., 1995; Zimmermann et al., 2001]. Fibroblast-specific proteins were detected by Western blotting, FACS analysis for surface markers, and/or immunocytochemistry. The cells were seeded in tissue culture flasks, and cultured until confluence in DMEM supplemented with 10% FBS and antibiotics at 37°C in a humidified atmosphere of 5% CO_2/95% air. Additionally, HSF were incubated in fresh medium containing 0.5–1% FBS for 24 h before the experiments and only second or third passaged HSF were used. HEK293T cells were purchased from American Type Culture Collection (ATCC, Rockville, MD) and were grown in DMEM supplemented with 10% FBS, penicillin (100 units/ml) and streptomycin (100 µg/ml) at 37 °C in a humidified atmosphere with 5% CO_2/95% air.

PhosphoScan™ PROTEOMIC ANALYSIS

Cellular protein was extracted into RIPA buffer (50 mM Tris–HCl, pH 7.4, 150 mM NaCl, 2 mM EDTA, 1 mM PMSF, 10 µg/ml each of aprotinin, leupeptin, and pepstatin, 1% NP-40, 1 mM sodium orthovanadate and 1 mM NaF) from control and 10 min PGE_2-treated HSF, sonicated at 15 W output for 25 s and centrifuged 15 min at 20,000g to remove insoluble material. Equal amounts (16.0 ± 0.2 mg) of total cleared proteins from treated and untreated samples were reduced, carboxamidomethylated and digested with endoproteinase GluC. Peptides were separated from non-peptide material by solid-phase extraction with Sep-Pak C18 cartridges. Lyophilized peptides were re-dissolved and phospho-peptides were isolated using a slurry of immobilized phosphorylated PKA substrate motif rabbit monoclonal antibody (Cell Signalling Technologies, Waverly, MA. CST # 9624). Peptides were eluted from the antibody coupled-resin into a total volume of 100 µl in 0.15% TFA. Eluted peptides were concentrated with PerfectPure C18 tips and digested using ProteoGenBioDiges Tips (10 µl) immediately prior to LC-MS analysis.

Peptides were loaded onto a 10 cm × 75 µM PicoFrit capillary column packed with Magi C18 AQ reversed-phase resin. The column was developed with a 45-min gradient of acetonitrile in 0.125% formic acid delivered at 280 nl/min. Tandem mass spectra were collected with an LTQ-Orbitrap hybrid mass spectrometer, using a top-ten method, dynamic exclusion repeat count of 1 and a repeat duration of 30 s. MS spectra were collected in the Orbitrap component of the mass spectrometer and MS/MS spectra were collected in the LTQ. MS/MS spectra were evaluated using TurboSequest in the Proteomics Browser Package and the following parameters: peptide ion mass tolerance, 2.5 Da; fragment ion mass tolerance, 1.0 Da, maximum number of differential amino acids per modification, 4; parent ion mass type, monoisotopic; fragment ion mass type, monoisotopic; maximum number of internal cleavage sites, 4; neutral losses of water and ammonia from b and Y ions were considered in the correlation analysis and the proteolytic enzyme was specified. Searches were performed against the NCBI human database and containing 34,180 protein sequences, in both forward and reversed sequence directions. The false positive assignment rate was approximated by taking the ration of the reversed database assignments to the forward database assignments after filtering the initial SEQUEST search results based on XCorr (>1.5), mass accuracy (±10 ppm) and on the presence of the expected sequence motif {(K/R) K/R X(s/t)} or {(K/R)X(s/t)}. The mass accuracy range was narrowed further based on the XCorr-mass error plot for each experiment. The average false positive assignment obtained from the SEQUEST search of the four LC-MS/MS experiments in this study was determined to be 3% [Moritz et al., 2010].

PREPARATION OF CELL EXTRACTS, IMMUNOPRECIPITATION, AND WESTERN BLOTTING

Fifty to 100 µg of cellular protein extracted into RIPA buffer or hot SDS–PAGE loading buffer, from control and treated cells, were subjected to SDS–PAGE through 8–10% gels (16 cm × 20 cm, final concentration of acrylamide) under reducing conditions, and transferred onto nitrocellulose membranes (GE Healthcare Amersham Pharmacia Biotech, Piscataway, NJ). Following blocking with 5% BLOTTO for 2 h at RT and washing, the membranes were incubated overnight at 4°C with the primary antibody in TTBS containing 0.25% BLOTTO. The second antibody-HRP conjugate (Cell Signalling Technologies, Danvers, MA; 1:10,000 dilution) was subsequently incubated with membranes for 1 h at RT, washed extensively for 30–40 min with TTBS, and a final rinsing with TTBS at RT. Following incubation with an ECL chemiluminescence reagent (Amersham Pharmacia Biotech), membranes were prepared for autoradiography, exposed to Kodak (Rochester, NY) X-Omat film, and subjected to digital imaging system (Alpha G-Imager 2000 Canberra Packard Canada, Mississauga, Ontario, Canada) for semi-quantitative measurements. The following rabbit antibodies were used: phospho-(S) PKC substrate (motif R/K-X-S-Hyd-R/K); phospho-(S) MAPK/CDK substrate (motif K/R-S-P-X-K/R); phospho-(S/T) ATM/ATF substrate (motif Hyd-S/T-Q); phospho (S/T) PKA substrate (motif R-R-X-S/T); phospho (Ser/Thr) AKT substrate (motif R/K-X-R/K-X-X-S/T); phospho-MYPT1 (T853); phospho-paxillin (Tyr118); and phospho-myosin light chain kinase 2 (S19) (Cell Signalling Technologies). Rabbit anti-human antibodies against actin, ROCK2, and PKAcat subunit were products of AbCAM (Cambridge, MA). For immunoprecipitation of ROCK2, transfected cells were lysed in RIPA buffer and lysates were pre-cleared prior to immunoprecipitation with anti-ROCK2 antibody (1 µg/mg protein) at 4°C overnight. Immunoprecipitated proteins were resolved and detected by Western analysis.

PLASMIDS AND TRANSFECTION EXPERIMENTS

Transient transfection experiments for reporter analysis were conducted in 6–12 well cluster plates as previously described [Faour et al., 2005; Zhai et al., 2010] using FuGENE6™ (Roche Applied Science, Indianapolis, IN) or Lipofectamine 2000 (Invitrogen™) according to the manufacturers' protocols with cells at 30–40% confluence. Cells were re-exposed to a culture medium with 1% FBS for 2 h prior to the addition of the biological effectors. Transfection efficiencies were controlled in all experiments by co-transfection with a pHSV-TK-driven Renilla luciferase construct (Promega Corp., Madison, WI). Luciferase values, expressed as enhanced relative light units, were measured in a Lumat LB 9507 luminometer (EG&G, Stuttgart, Germany) and normalized to the levels Renilla luciferase activity and cellular protein (bicinchoninic acid procedure; Pierce). In signal transduction pathway reporting systems (Stratagene/ Agilent Technologies, Inc., Mississauga, ON), a reporter plasmid, containing the 17 bp ($5\times$) Gal4 DNA binding element (UAS) fused to a TATA box upstream from the luciferase gene (pFR-LUC) was co-transfected with a construct containing the trans-activation domains of transcription factors (e.g. pFA-CREB/ATF1) fused to GAL4 DNA binding domain and driven by a CMV promoter. Plasmids expressing the active PKA catalytic subunits and active Akt or Raf1 were used to confirm the transactivation domain targeting of CREB. A construct expressing a dominant-negative mutant of PKA regulatory subunit Ia (dnPKA RIa) was generated by subcloning a PCR fragment of the published sequence cDNA into the pcDNA 3.1 vector. The mutant harbours three mutations at E200, D324 and H332, rendering the subunit incapable of binding cAMP and releasing the catalytic subunits [Clegg et al., 1992].

The full-length ROCK2/KIAA0619 (GenBank Accession No. O75116) expression construct was kindly provided by the Kazusa DNA Research Institute (Chiba, Japan) and was originally inserted at a SalI-Not1 site of the pBluescript II SK (+) vector. The cDNA was subcloned into pcDNA3.1 expression vector and S1379A (Ser → Ala) mutant was constructed from the wild-type (wt) ROCK2 expression vector using the QuikChange kit (Stratagene, La Jolla, CA) as previously described [Zhai et al., 2010]. The following primers were used: sense, 5′-CCA GTC TAT TAG ACG GCC AGC TCG ACA GCT TGC CCC AAA CAA ACC-3′; antisense, 5′-GGT TTG TTT GGG GCA AGC TGT CGC GAT GGC CGT CTA ATA GAC TGG-3′. Base-pair substitutions were verified by double DNA sequencing. The wt and mutated plasmids were transfected using Amaxa Nucleofector technology (Lonza, Walkersville, MD) with the Human Dermal Fibroblast Nucleofector Kit. The Nucleofector Device was set at program U-23 for synovial fibroblasts: each cuvette that underwent nucleofection contained 1 10⁶ cells suspended in Nucleofector Solution, to which 2 μg of plasmid DNA were added. Between 0.2 and 0.5 μg of pCMV-β-gal, a β-galactosidase reporter vector under the control of CMV promoter (Stratagene), was used as a transfection control.

IMMUNOCYTOCHEMISTRY AND CONFOCAL MICROSCOPY

For all fluorescence imaging, an LSM 510 META confocal microscope (Carl Zeiss MicroImaging GmbH, Jena, Germany) was employed. Cells were seeded onto sterile coverslips and allowed to grow for 48 h prior to fixation. Following fixation with 4% formaldehyde in PBS, coverslips were incubated in 50 mm NH₄Cl in PBS to quench remaining aldehyde groups. After washing three times with PBS, cells were permeabilized using 0.1% saponin in PBS. Non-specific antibody binding sites were blocked using 0.2% fish skin gelatin in PBS. Cells were incubated with either anti-phosphopaxillin (Tyr118), anti phosphomyosin light chain 2 (S19), or anti-phospho PKA motif [(K/R-(K/R)X(s/t)]. Primary antibodies were revealed using Alexa Fluor 488 goat anti-rabbit and Alexa Fluor 594 chicken anti-mouse secondary antibodies. Cells were mounted on glass slides using Mowiol mounting medium with anti-fade agent (1,4-diazabicyclo-[2.2.2]octane) prior to microscopy. Alexa Fluor 488 was excited by the 488-nm argon ion laser, and the fluorescence was collected using a BP505-530 emission filter, whereas Alexa Fluor 594 was excited by the 543-nm HeNe laser line, and the fluorescence was collected using an LP560 emission filter. All images were acquired using a Plan-Apochromat ×63/1.40 oil differential interference contrast objective in sequential scanning (multitrack) mode with the pinholes set to obtain an optical section of about 0.8 μm in both channels (∼1 Airy unit) [Kartberg et al., 2010].

STATISTICAL ANALYSIS

All results were expressed as the mean ± SD or mean and the coefficient of variation (CV) of 3–5 separate experiments as indicated. Transfection experiments were performed in triplicate. Statistical treatment of the data was performed parametrically (Student's t-test) or by non-parametric (Mann–Whitney) analysis if Gaussian distribution of the data could not be confirmed. Significance was acknowledged when the probability that the null hypothesis was satisfied at <5%.

RESULTS

PHOSPHOPROTEOMIC ANALYSIS OF PGE₂/GPCR/PKA PHOSPHORYLATED SUBSTRATES IN HSF

Preliminary experiments were conducted to screen for Ser/Thr kinase substrates by Western analysis using antibodies to kinase-specific phosphorylation motifs (see the Experimental Procedures Section, data not shown). We observed primarily PKA-substrate phosphorylation patterns (list also included MAP kinase, PKC, CDK, ATM, Akt) that was time (Fig. 1A) and concentration dependent. Densitometric analysis of multiple blots revealed that the EC₅₀ was 29 ± 4 nM while the onset was rapid (s), reached a zenith at 10–15 min and was stable for up to 30 min. Activating cAMP by forskolin treatment mimicked the effects of PGE₂ that were reversed by the PKA inhibitor H89 (Fig. 1B). In addition, since elevations in [cAMP]ᵢ, as for example under PGE₂ stimulation, can modulate EPAC activation with subsequent downstream Rap1 GTPase and MAP kinase signalling, we used a synthetic cAMP mimic (8cPT-cAMP) known to target EPAC, which was without effect. In support, the MEK1 inhibitor PD58059 did not influence the actions of PGE₂ or 8cPT-cAMP (data not shown). Two-dimensional gel electrophoresis and Western analysis confirmed the substrate size distribution, array and acidic nature of most of the PKA phosphorylated substrates (Fig. 1C). An EP2 agonist stimulated a response closely related to PGE₂ in contrast to that of the EP4 agonist (Fig. 1D). EP1 and EP3 agonists did not affect the PKA phosphorylation profile (data not shown). Confocal analysis revealed that, in
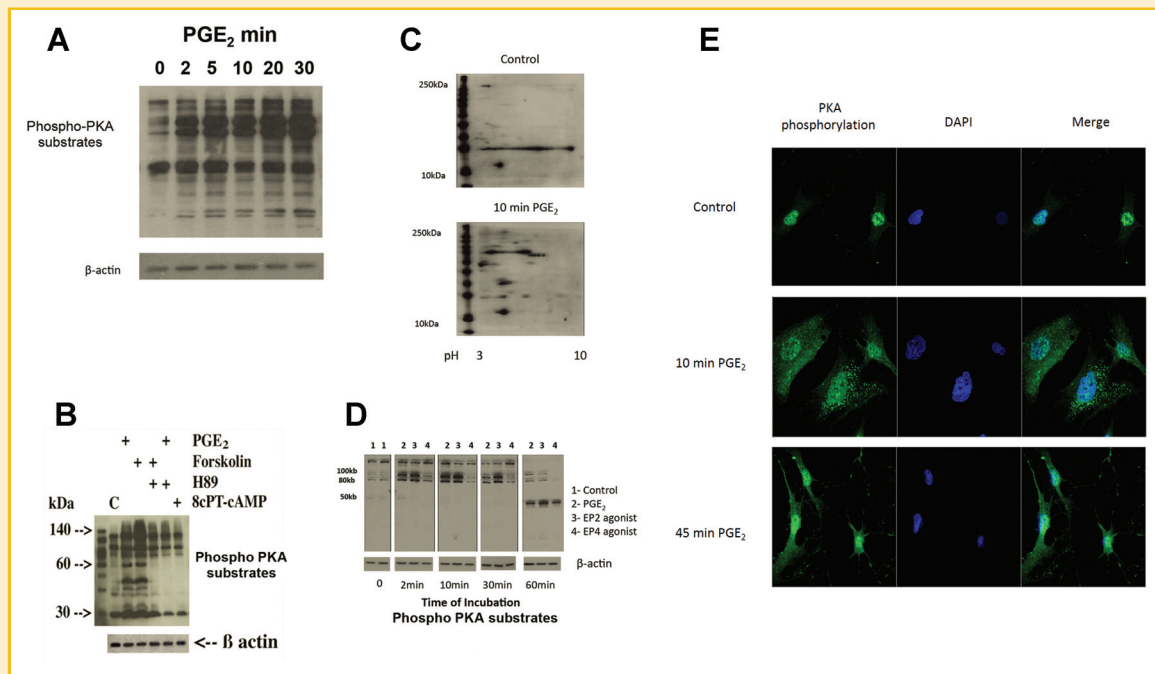
Fig. 1. Preliminary analysis of PGE$_2$–dependent substrate phosphorylation: In (A), cultured HSF were synchronized in DMEM 1% FBS and then treated with 100 nM PGE$_2$ for 0, 2, 5, 10, or 30 min or, as in (B), with 10 μM of forskolin or 100 nM of PGE$_2$ for 10 min in the presence or absence of H89; cells were also exposed to 8cPT–cAMP (10 μM). Total cell lysates were subjected to 1– (A and B) or 2– (C) dimensional Western analysis using a phospho(S/T)PKA substrate antibody and the β–actin antibody as a loading control as described in the Experimental Procedures Section. In (D), cells cultured as in (A), were treated for 0, 2, 10, 30, or 60 min with 100 nM PGE$_2$, 100 nM EP2 agonist (butaprost), or 100 nM EP4 agonist (L–902688) and total protein cell extracts were subjected to Western analysis using the phospho(S/T)PKA substrate and β–actin antibody. In (E), HSF were seeded on 6 well glass microscope slides and cultured for 24 h in complete medium and then incubated for 2–4 h in DMEM + 1% FBS prior to the addition of 100 nM PGE$_2$ for 0, 10, and 45 min. Cells were fixed, permeabilized and subjected to immunocytochemistry using the phospho–(S/T)PKA substrate antibody. Confocal microscopy localized the effect of PGE$_2$ on PKA substrates (green) and DAPI was used to stain the nucleus.

untreated cells, most of the immunoreactive substrates were nuclear while PGE$_2$ treatment resulted in pan cellular phosphorylation patterns (Fig. 1E). Phosphopeptide analysis (see the Experimental Procedures Section) identified a number of known PKA substrates as well as non-redundant targets under PGE$_2$/GPCR control; some examples are shown in Table 1. Many of the proteins were associated with the cellular cytoskeleton and so presumably had a role in cellular structure and functional dynamics (e.g. cytoskeletal contraction and cell migration); in this regard, we identified a unique non-redundant, heavily phosphorylated (>30-fold) site on rho-associated coiled coil-containing kinase 2 (ROCK2) at S1379, becoming our target for cytoskeletal changes.

PGE$_2$ CAUSES RAPID AND SUSTAINED MORPHOLOGICAL CHANGES IN HSF

To address the role that PGE$_2$-induced phosphorylated substrates (as monitored by Western/proteomic analysis) have on cytoskeletal functional changes, we conducted, in a preliminary fashion, light phase-contrast microscopy to observe cellular morphology over the same time course. PGE$_2$ stimulated a rapid morphological change in fibroblasts as early as 10 min and persisted for some 90 min with distinct features such as the development of pseudopodial extensions, which radiated from the cell in a star-like shape (Fig. 2A). Parenthetically, the AHNAK nucleoprotein/desmoyokin, which functions in pseudopodia to organize the actin cytoskeleton

TABLE 1. Phosphopeptide Analysis: Known PKA substrates As Well As Non-Redundant Targets Under PGE$_2$ Control

Protein name		Site	Peptide	Raw intensity		Ratio
				Control	PGE$_2$	
FLNA	Filamin A, alpha isoform 2	#2336	RLT*VSSLQE	556,217	24,345,786	43.8
HSP20	Heat shock protein 20	#16	RAS*APLPGLSAPGR	1,467,758	46,886,030	31.9
MENA	Enabled homolog isoform a	#265	RIS*SAAAPASVE	37,742	832,110	22.0
ARHGEF17	Rho guanine nucleotide exchange factor 17	1717, 1725	RSS*HGSFTRGS*LE	20,000	159,251	8.0
DOCK7	Dedicator of cytokinesis 7	439, 440	RNS*S*IVGRRSLE	20,000	365,818	18.3
ROCK2	Rho-associated coiled-coil containing kinase 2	1379	RPS*RQLAPNKPS	39,312	1,217,349	31.0
AHNAK	AHNAK nucleoprotein isoform 1	158	RVT*AYTVDVTGRE	473,966	17,612,019	37.2
AHNAK	AHNAK nucleoprotein isoform 1	177	DVTGREGAKDIDISS*PE	29,301	578,689	19.7

#, Published site; *, phosphorylated site.

and the architecture of the cell membrane, was phosphorylated 37-fold at site T158 (R_{156}Vphospho-TAYTVDVTGREAKDDISSPE; extracted phospho-ion chromatogram raw intensity data; control, 473,966 vs. PGE_2, 17,612,019, n = 2 determinations). Under similar conditions, the adenylyl cyclase activator forskolin and the ROCK2 inhibitor Y27632, induced rapid and persistent morphological changes similar to PGE_2 (Fig. 2A). In this connection, we examined intracellular structural components such as actin filaments using phalloidin staining under confocal microscopy. In untreated HSF, we observed actin in the formation of filament strands spanning the cell body of what is typically a normal cytoskeleton (Fig. 2B). In contrast, PGE_2 treatment resulted in a marked disassembly of the actin filamentous skeleton, accounting for the change in cell shape and reduction in cytoplasmic volume.

PGE_2-DEPENDENT EFFECTS ON MYOSIN LIGHT CHAIN (MLC) AND MYOSIN LIGHT CHAIN PHOSPHATASE (MYPT-1) PHOSPHORYLATION, AND STRESS FIBRE FORMATION

Cytokine/growth factor activation of ROCK2 results in the phosphorylation of a number of proteins associated with cytokinesis, smooth muscle contraction (e.g. myosin light chain kinase/phosphatase), MLC-induced actin bundling, the formation of actin stress fibres (e.g. α-smooth muscle actin) and FAs (e.g. phospho-paxillin), processes critical to and characteristic of myofibroblasts. Inhibition of ROCK2 activity with the inhibitor Y27632 stimulated a rapid morphological change in HSF as early as 10 min and persisted for some 90 min as judged by light microscopy, as shown in Figure 2A; indeed these changes were concomitant with altered patterns of MLC phosphorylation (Fig. 2C) and α-smooth muscle actin expression (data not shown). PGE_2 mimicked these effects both on a temporal and qualitative basis and the PGE_2/GPCR blockade of MLC phosphorylation was observed to occur within minutes (Fig. 2C). To visualize the functional changes in MLC phosphorylation, stress fibre/actin filament formation and cellular morphology, we conducted confocal microscopy as shown in Figure 2D. PGE_2-induced dephosphorylation of MLC was associated with the loss of an intact filamentous actin cytoskeleton as shown by the changes in phalloidin staining patterns and the overlap visualization. Phosphorylation of MLC at S19 was associated with changes in MYPT phosphorylation (deactivation) at T853 under LPA/TGF-β (cytokine) induced conditions as shown in Figure 2E. The deactivation/phosphorylation of the MYPT-1 subunit of protein phosphatase-1 (PP-1) was blocked by co-incubations with PGE_2 (Fig. 2E).
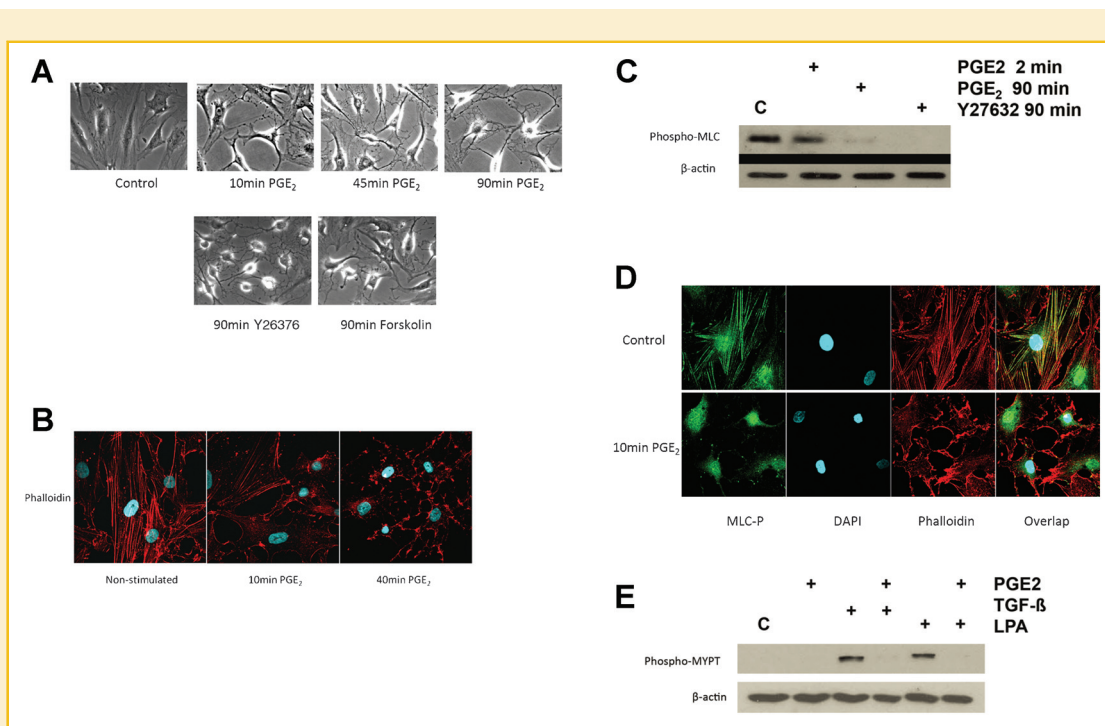
Fig. 2. PGE_2 causes rapid and sustained changes in fibroblast morphology: Effects on myosin light chain (MLC) and myosin light chain phosphatase (MYPT-1) phosphorylation, and stress fibre formation. In (A), human synovial fibroblasts (HSF) were seeded in 6-well plates and cultured for 24 h in complete medium and then incubated for 2–4 h in DMEM + 1% FBS prior to the addition of 100 nM PGE_2 for 0 (control), 10, 45, and 90 min, or for 90 min with 10 μM of the adenylate cyclase activator forskolin or 10 μM of the ROCK2 inhibitor Y27632. Light phase-contrast microscopy was used for capturing morphological changes. In (B) and (D), HSF were seeded in 6-well glass microscope slides for 24 h in complete medium and then incubated for 2–4 h in DMEM + 1% FBS prior to the addition of vehicle (control) or 100 nM PGE_2 for 10 min (B and D) and 40 min (B). Cells were then fixed and confocal microscopy was used to stain for nuclei using DAPI (blue) and actin filaments with phalloidin (red) (B). The state of MLC phosphorylation with untreated and treated cells was determined by immunocytochemistry using phospho-MLC (S19) antibody while the structure of stress fibres was visualized by phalloidin staining and the nucleus with DAPI (D). The influence of MLC phosphorylation on stress fibre integrity was visualized in the overlap image (yellow). Images are representative of >90% of the total population of cells in three separate preparations; bar scale 15 μm. In (C) and (E), HSF were cultured as described above and treated with vehicle (control), PGE_2 or Y27632 as indicated (C), or with combinations of 10 ng/ml TGF-β, 10 nM LPA and/or 100 nM PGE_2 for 10 min (E). Cells were extracted for total protein and subjected to Western analysis using anti-phospho MLC (S19), anti-phospho MYPT-1 (T853) and anti-β-actin antibodies as described in the Experimental Procedures Section.

In order to characterize on a preliminary basis the mechanism of PGE$_2$ signalling on the ROCK2 substrate MLC, we used specific EP2/EP4 agonists in co-incubations under basal and TGF-β-induced conditions; only the EP2 agonist mimicked the effects of PGE$_2$ and forskolin (Fig. 3A). Furthermore, PGE$_2$ suppression of cytokine-induced MLC/MYPT-1 phosphorylation was reversed in the presence of PKA inhibitors H89 and KT-5720 (Fig. 3B). We also observed no effect of the cAMP mimic (8cPT-cAMP) on MLC/MYPT-1 phosphorylation under basal or TGF-β-induced conditions.

ROLE OF PKA IN PGE$_2$-DEPENDENT ROCK2 AND CREB-1 PHOSPHORYLATION

Although S1379 of ROCK2 is part of a high stringency PKA motif (see the Experimental Procedures Section) in cell-free systems, we conducted additional experiments to verify the specificity in cell culture models. HEK293T cells were used to express high levels of PKA and ROCK2 in order to study the functional and molecular dynamics/interactions between them. As shown in Figure 4A, the phosphorylation of S1379 induced by PGE$_2$ and forskolin was mimicked by overexpression of a PKA catalitic (PKAcat) expression

Fig. 3. EP2 and PKA mediate PGE$_2$-dependent effects on the phosphorylation state of ROCK2 primary substrates, MLC and MYPT-1. In (A), HSF were seeded into 6-well plates and cultured for 24 h in complete medium and then incubated for 2–4 h in DMEM + 1% FBS prior to the addition of vehicle (control), 10 ng/ml TGF-β, 100 nM PGE$_2$, 100 nM EP2 agonist (butaprost), 100 nM EP4 agonist (L-902688), or 10 μM forskolin for 60 min as indicated in the figure. Total protein cell extracts were subjected to Western analysis using antiphospho-MLC (S19) and anti-β-actin antibodies. In (B), HSF were cultured as above and then treated with 100 nM PGE$_2$ and/or 10 ng/ml TGF-β in the presence or absence of PKA inhibitors H89 (10 μM), KT-5720 (2 μM), or the EPAC activator 8cPT-cAMP (10 μM) for 60 min after which time the cells were extracted for total protein and subjected to Western analysis using anti-phospho MLC (S19), anti-phospho MYPT-1 (T853) and anti-GAPDH antibodies as described in the Experimental Procedures Section.

vector but reversed when a dominant negative mutant of the PKA regulatory Ia subunit (dnPKArI) was overexpressed in PGE$_2$/ forskolin treated cells. The EPAC activator 8cPT-cAMP was without effect compared to controls although a combination of forskolin and Ro-20-1724, a type IV cAMP-dependent phosphodiesterase inhibitor, produced a robust increase in ROCK2 S1379 phosphorylation. Ro-20-1724 alone was essentially without effect; no increase in [cAMP]$_I$ was observed in HSF (data not shown) in contrast to other cell phenotypes [Faour et al., 2005].
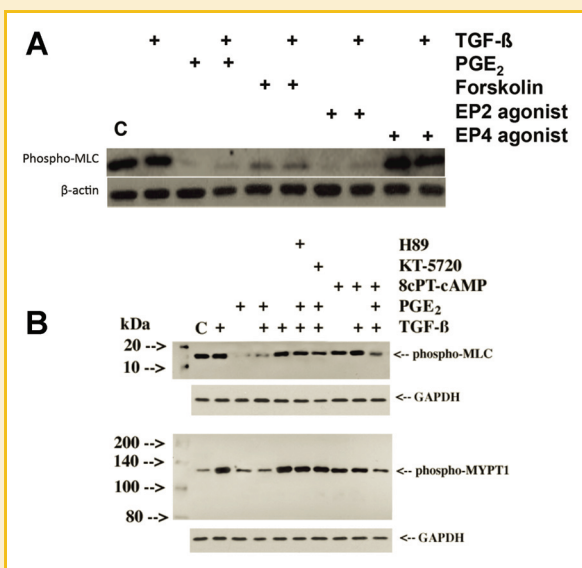
We pursued these experiments with immunoprecipitation/pull down experiments of overexpressed PKAcat, and ROCK2 wt or ROCK2 S1379A mutant in kinase assays. We observed that only the wild-type expressed protein was phosphorylated specifically at S1379 by the kinase activity of PKAcat (Fig. 4A and B).

In order to verify for productive functional changes associated with PKA-dependent phosphorylation as well as a positive control for the sensitivity/specificity of our phosphoproteomic analysis, we observed that the substrate CREB-1 (phospho S133) (Fig. 4C) could transactivate a responsive-CRE luciferase reporter (Fig. 4D); over expression of a dominant negative construct of CREB (S133A) abrogated the PGE$_2$-dependent induction of the luciferase reporter (Fig. 4D); forskolin and overexpressed PKAcat mimicked PGE$_2$-dependent effects.
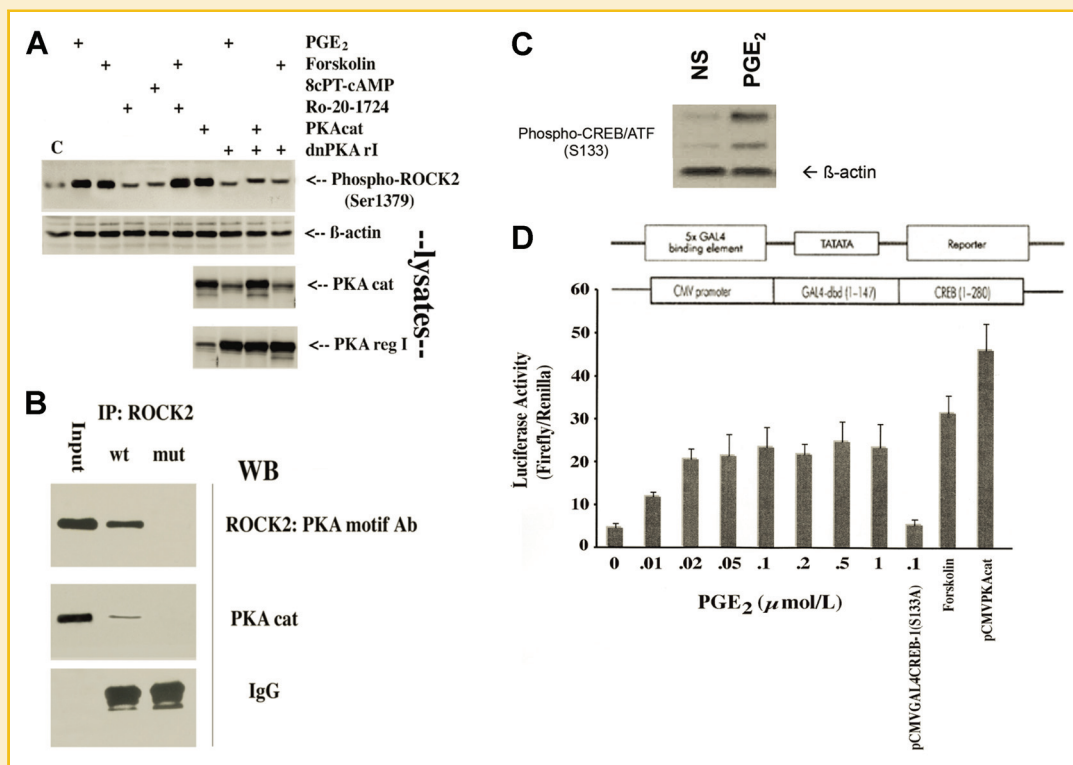
PGE$_2$ INHIBITS ROCK2 ACTIVITY THROUGH S1379 PHOSPHORYLATION: ROLE IN STRESS FIBRE DISASSEMBLY AND CYTOSKELETAL ULTRASTRUCTURE

The data thus far suggested that PGE$_2$/PKA induced phosphorylation of ROCK2 S1379 (either under basal culture conditions or induced) was inhibitory. As such, we pursued this notion further by investigating downstream substrates/targets of ROCK2 in HSF under control conditions or treated with PGE$_2$ with cells overexpressing wt ROCK2 or a ROCK2 S1379A mutant construct. Forced over-expression of the mutant ROCK2 protein abrogated to a very significant extent PGE$_2$-dependent effects on MLC and MYPT phosphorylation (Fig. 5A–C). Furthermore, with regards to FA formation, PGE$_2$ strongly inhibited basal paxillin phosphorylation at T118 as judged by confocal microscopy and Western analysis (Fig. 6A,B). Overexpression of mut S1379A ROCK2, but not wt ROCK2, abrogated PGE$_2$-induced inhibition of paxillin phosphorylation (Fig. 6C).

If ROCK2 activity controls actomyosin and stress fibre formation and S1379 phoshorylation (e.g. by PGE$_2$) compromises this activity, then overexpression of S1379A ROCK2 should for the most part mitigate any PGE$_2$ effects on cytoskeletal architecture. Indeed, as shown in Figure 7, PGE$_2$ treatment of cells stably over expressing the mutant was largely without discernible effects (bright field and confocal microscopy). Interestingly, while WT ROCK2 overexpression did not appear to effect cellular cytoskeletal architecture under basal culture conditions, the mutant induced extensive stress fibre formation as judged by confocal microscopy, relevant to the wide bodied cells visualized by light microscopy. Figure 8 summarizes a plausible mechanism by which PGE$_2$ modulates stress fibre formation, focal adhesions and cellular architecture under cytokine/growth factor/mechano control.

Fig. 4. Role of PKA in PGE$_2$–dependent ROCK2 and CREB-1 phosphorylation. In (A), quiescent HEK293T cells were treated with or without 100 nM PGE$_2$, 10 μM forskolin, 20 μM Ro-20-1724, 10 μM 8cPT-cAMP, or forskolin + Ro-20-1724 for 10 min. Alternatively, cells were transfected with 50 ng of a construct expressing the PKA catalytic subunit (PKAcat) or the dominant negative mutant of the PKA regulatory Ia subunit (dnPKArI) alone or in co-transfection. In addition, cells transfected with 50 ng of dnPKArI, were treated for 10 min with either 100 nM PGE$_2$ or 10 μM forskolin. Treated cells were lysed in RIPA buffer and equal volumes/protein concentrations immunoprecipitated with a specific Phospho–ROCK2 (Ser1379) antibody and processed for Western analysis using the phospho-(S/T)PKA substrate antibody. Lysates were also screened for ß-actin, PKAcat and dnPKArI content by Western analysis. In (B), HEK293T cells were transfected with 100 ng each of the ROCK2 wt expression vector or the S1379A ROCK2 mutant, and 50 ng of PKAcat. Cells were then treated with 100 nM PGE$_2$ for 10 min after which time lysates were bead immunoprecipitated with antibodies against PKAcat and ROCK2. Precipitants were mixed together with reaction buffer for an additional 30 min, washed and subjected to Western analysis using the phospho-(S/T)PKA substrate antibody. Lysates were also screened for ROCK2 and PKAcat by Western analysis. In (C), quiescent HSF were treated with or without 100 nM PGE$_2$ after which time the cells were lysed and subjected to Western analysis for phospho–CREB/ATF (S133) and β-actin using specific antibodies as described in the Experimental Procedures Section. In (D), cells were co-transfected with 1 μg of 5X GAL4–TATAA-luciferase reporter and 50 ng of Gal4-CREB-1 construct for 16 h in complete medium after which time the cells received a change of medium and treated with or without increasing concentrations of PGE$_2$ or 50 μM forskolin for 6 h. In addition, cells were co-transfected with an additional 100 ng of a Gal4-CREB (S133A) mutant in the presence of 100 nM PGE$_2$ or 50 ng of a construct expressing the PKA catalytic subunit (PKAcat). Cells were then lysed and luciferase activity was measured as described in the Experimental Procedures Section.

DISCUSSION

The regulation of myofibroblast differentiation is a critical control point in normal and pathological tissue repair responses. In fibrotic diseases, this network becomes dysregulated by processes that remain ill defined, leading to the accumulation of myofibroblasts and potentially fibrosis. The most clearly defined molecular events leading to myofibroblast differentiation include both mechanical forces exerted by components of the ECM that are mediated by cellular mechanoreceptors, and growth factors (e.g. TGF-β) that initiate post-receptor activation of intracellular signalling cascades [Butcher et al., 2009]. For example, the synovial fluid of rheumatoid arthritis patients is able to induce a myofibroblast phenotype through a TGF-β-dependent mechanism [Song et al., 2010]. However, few factors/processes that inhibit myofibroblast differentiation have been identified and even less is known regarding their

signalling pathways. In this regard, we studied the potentially anti-fibrotic effects of the PGE$_2$/EP/GPCR receptor system on the fibroblast to myofibroblast phenotype with the goal of elucidating signalling pathways that mediate such responses at the molecular level [Kolodsick et al., 2003; Sandulache et al., 2007; Thomas et al., 2007]. We chose to employ phosphoproteomic techniques because we required a sensitive, precise and quantitative procedure to identify substrates and signalling intermediates downstream of ligand-receptor binding in addition to potential cross-talk.
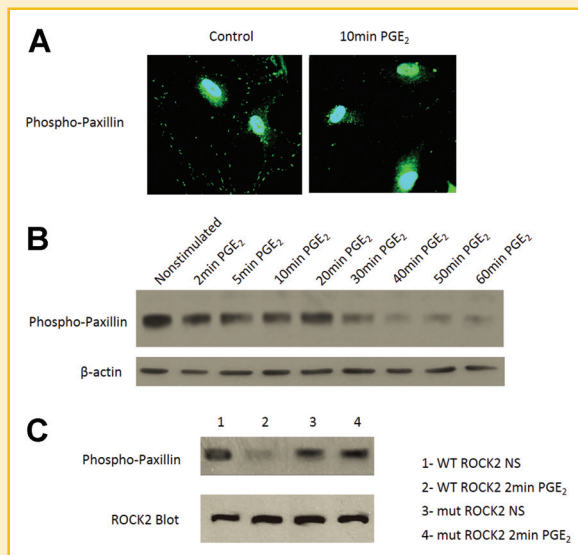
The PGE$_2$/EP/cAMP/PKA signalling cassette has been implicated in stress fibre disassembly and changes in cellular morphology [Dong et al., 1998; Kolodsick et al., 2003; Thomas et al., 2007], although substrate specificity and functional changes in substrate activity due to post-translational modifications remain largely unexplored. Although our large number of phosphorylated substrates have structural functions and almost certainly work together
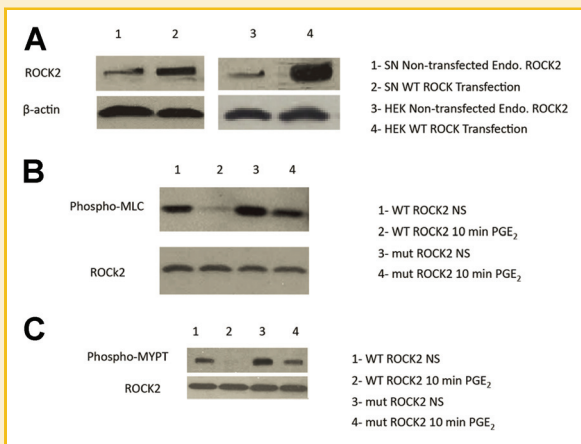
Fig. 5. PGE$_2$ induced PKA–phosphosite S1379 ROCK is inhibitory: HSF and HEK293T cells were transfected with 2 µg each of wild–type or mutant (S1379A) ROCK2 vectors as described under the Experimental Procedures Section, and cells were cultured further for 24–48 h in complete medium. In (A), transfection efficiency was monitored in part by Western analysis of overexpressed proteins using specific anti–ROCK2 and anti–β–actin antibodies. Transfected HSF were rendered quiescent and synchronized in DMEM 1% FBS for 4 h. Cells were then treated with or without 100 nM PGE$_2$ for 10 min. Cell extracts were blotted for phospho–MLC (B) and phospho–MYPT (C) to evaluate putative ROCK2 activity. Protein loading was controlled by blotting for ROCK2.

Fig. 6. PGE$_2$ induced PKA phosphosite S1379 ROCK affects downstream adhesion complex assembly: Immunolocalization and the mature state of focal adhesions were analysed by the phosphorylation status of paxillin using an anti–phospho–(Tyr118) Paxillin antibody. In (A), HSF were plated on 6–well glass microscope slides for 24 h in complete medium and then 4 h in DMEM 1% FBS. Cells were either treated or not with PGE$_2$ for 10 min, followed by fixation and permeabilization as described in the Experimental Procedures Section. Phospho–(Tyr118) Paxillin antibody (green) was detected by confocal microscopy. In (B), cells cultured as in (A), were treated for 0–60 min with 100 nM of PGE$_2$ and total protein cell extracts were subjected to Western analysis using antiphospho–(Tyr118) Paxillin antibody. In (C), HSF were transfected with 2 µg each of wild–type or mutant (S1379A) ROCK2 vectors as described under the Experimental Procedures Section, and cells were cultured further for 24–48 h in complete medium. Cells were then treated with or without 100 nM PGE$_2$ for 10 min and extracted proteins were subjected to Western blot analysis of phospho–Tyr118 paxillin. Protein loading was controlled by blotting against β–actin (B) and ROCK2 (C).

in a coherent network, we decided to investigate the RhoA/ROCK2 pathway as it is primarily responsible for the formation of stress fibres, such that contractile force signalling buttresses adhesion to the ECM. The latter process also involves the maturation of FAs [Pasapera et al., 2010]. One could assume that ROCK2 inhibition and subsequent loss in stress fibres would also be reflected in the proportional loss of FAs. Indeed, FA complexes involve a number of proteins that were phosphorylated in our phosphoproteomic screen (Table 1) (e.g. Mena (aka Ena), ARFGAP1, and GIT1) [Turner, 2000; Wozniak et al., 2004]. For these reasons we investigated the structural state of FAs after PGE$_2$ treatment and targeted Y118 of paxillin since phosphorylation of this site is essential for proper FA formation [Ballestrem et al., 2006; Schneider et al., 2009; Pasapera et al., 2010]. Our results clearly showed that PGE$_2$ treatment signalled a decrease in FA assembly and adhesion and this was associated with a marked dephosphorylation of paxillin at Y118. This was coincident with the decrease in contraction probably the result of PGE$_2$–dependent dephosphorylation of MLC. Furthermore, our mutant S1379A ROCK2 had a higher signal of phospho–Y118 paxillin than the wild type, indicating that a lack of inhibition by phosphoS1379 of ROCK2 allows for continuous phospho–MLC contraction followed by reinforced adhesion through phospho–Y118 paxillin. Taken together, we propose that PGE$_2$ signals through PKA to phosphorylate ROCK2 at S1379 and inhibit its activation/phosphorylation of MLC; the latter process decreases contraction. This lack of contractile force causes dephosphorylation of paxillin Y118, resulting in the disassembly of FAs and decrease in adhesion. The latter mechanism requires further study particularly with regard to focal adhesion kinase (FAK), which is known to phosphorylate

paxillin at Y118 [Ballestrem et al., 2006; Schneider et al., 2009; Pasapera et al., 2010].

The loss in ROCK2–dependent phosphorylation at S19–MLC and T853–MYPT1 after PGE$_2$ treatment supports the notion that PGE$_2$ inhibits ROCK2 activity. To analyse the integrity of the actomyosin structure, immunocytochemistry indicated that unstimulated fibroblasts had phosphoS19–MLC colocalize with actin to form stress fibres, showing the activated phosphoS19 state of MLC to be functional. However, PGE$_2$ treatment of fibroblasts induced the loss of S19–MLC phosphorylation, and as a result, a loss of actin bundling into filaments. Therefore, PGE$_2$ inactivating MLC from linking actin into stress fibres would allow for the collapse of the fibroblast morphology.

In untreated fibroblasts, we observed actin in the formation of filament strands spanning the cell body of what is typical of a normal cytoskeleton. On the other hand, PGE$_2$ treatment resulted in the complete disassembly of a sound skeleton. It is the loss of this stability that would account for a rapid change in cell shape and deflated cytoplasm. Therefore, our data suggests that changes in
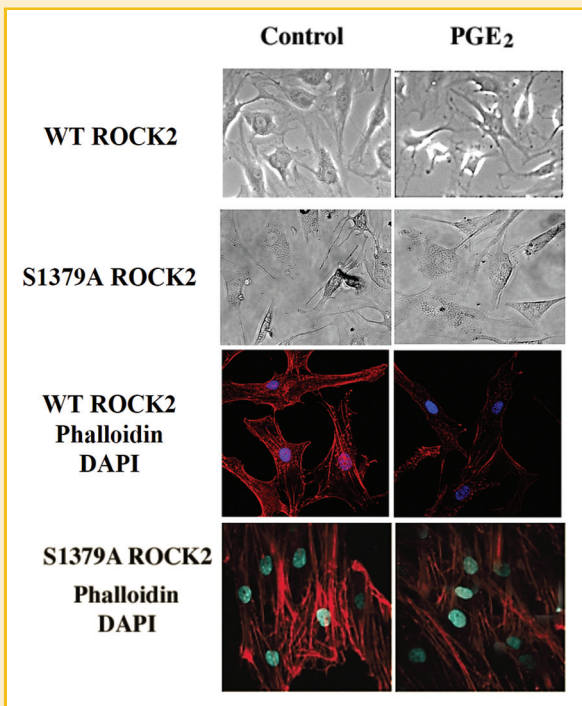
Fig. 7. Mutation at Ser1379 of ROCK2 protects from the cytoplasm deflation and pseudopod formation induced by PGE$_2$: HSF were stably transfected with 2 µg each of wild-type or mutant (S1379A) ROCK2 vectors as described under the Experimental Procedures Section, and cells were cultured further for 24–48 h in complete medium. Cells were then treated with or without 100 nM PGE$_2$ for 10 min. Light phase-contrast microscopy was used for capturing morphological changes while stress fibre formation was visualized by phalloidin staining (red); the nucleus was stained with DAPI.
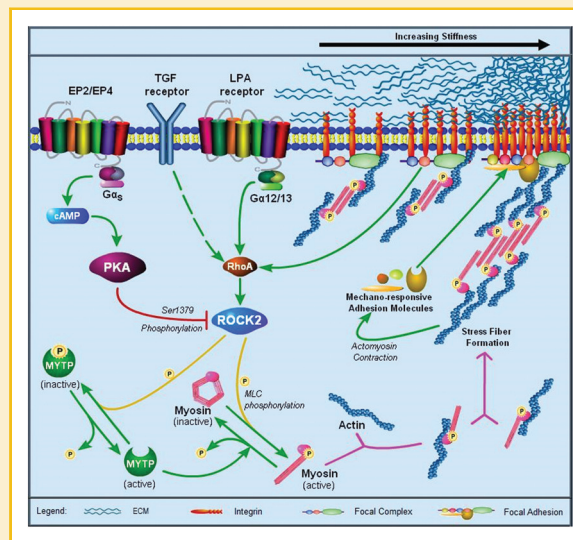
Fig. 8. Mechanical regulation through ROCK2: The Rho pathway can be activated by various cues, for example LPA binding to GCPR activation of G$\alpha_{12/13}$, a rigid ECM exerting force on the integrins that signal through focal complex molecules, and the less known pathway of TGF-β signalling. RhoA activates ROCK2, which subsequently activates myosin. It does so by phosphorylating MLC on S19, releasing its autoinhibition, and MYPT, which inactivates it from removing the activating phosphate of MLC. In its assembly competent form, phospho-myosin is able to bind actin and assemble into bipolar filaments with other phospho-myosin. Bipolar myosin filaments bind other actin filaments into bundles to form large structures of stress fibres. The motor domain of myosin then creates contraction that signals through adhesion molecules (i.e. paxillin) to cluster at focal complexes and mature into focal adhesions, reinforcing the linkage between the cytoskeleton and adhesion. The reversal occurs upon PGE$_2$ binding to EP2 and partly through EP4. These GPCRs increase the cAMP levels through Gα_s, which leads to PKA activation. PKA then phosphorylates ROCK2 at S1379 and inhibits its phosphorylation of myosin or MYTP, which in turn promotes MLC dephosphorylation. Dephosphorylated MLC keeps myosin in an inactive form and prevents its direct contribution of stress fibre formation and indirect FA maturation.

cellular morphology involve the PGE$_2$-induced PKA phosphorylation of our targeted cytoskeletal and adhesion proteins. The functional focus of our phosphoproteome on the cellular architecture was apparent by the drastic changes in cytoskeletal actin filaments and fibroblast morphology. The following selected PhosphoScan proteins from Table 1 provide a possible explanation to our confocal microscopy results. For instance S16 of HSP20 (HSPB6), a small heat shock protein that plays a role in cytoskeletal regulation [Dreiza et al., 2005], had a 31.9-fold increase in phosphorylation after PGE$_2$ treatment. It has been shown that PKA phosphorylation of HSP20 at Ser16 causes changes in morphology, loss of stress fibres, and a decrease in focal adhesion complexes, which ostensibly prevents contraction [Komalavilas et al., 2008]. Another cytoskeletal protein is filamin A, which was phosphorylated 43.8-fold more at T2336 and 2.9-fold more at S2152 after PGE$_2$ stimulation. Generally, filamins are actin-binding proteins that organize actin filaments into networks, act in structural roles in cell adhesion, and serve in subcellular targeting of signalling molecules [Stossel et al., 2001]. Specifically, phosphorylation of filamin A on S2152 regulates actin cytoskeletal changes [Woo et al., 2004]. Hence, we may hypothesize that our PGE$_2$-induced PKA phosphorylated sites on filamin are inhibitory so as to reflect the

cytoskeletal breakdown PGE$_2$ imposed on fibroblasts. One of the most substantially targeted peptides in our list turned out to be a cytoskeletal protein known as AHNAK, which was dually phosphorylated at T158 and S177 with a combined 56.9-fold increase upon PGE$_2$ treatment. AHNAK localizes in peripheral actin-rich pseudopodial domains and is critical for pseudopodial protrusion, actin cytoskeleton dynamics and cell migration. In fact, another distinct feature of our post-PGE$_2$ treatment was the development of pseudopodial extensions, which radiated from the cell in a star-like shape. Given that AHNAK functions in pseudopodial protrusion, our high fold difference in AHNAK phosphorylation provide a reasonable explanation to our microscopy results, suggesting that the phosphosites of AHNAK are activating sites. The emphasis that PKA had on these structural proteins in regards to morphological changes is consistent with previous data indicating that cAMP/PKA affects actin cytoskeletal dynamics and migration [Dong et al., 1998; Howe, 2004].

In order to substantiate our novel PGE$_2$-induced PKA phosphosite S1379 on ROCK2 with our PGE$_2$ inhibition of ROCK2 activity data, we used a number of approaches including PKA chemical inhibitors, PKA cat and dnPKA RIa overexpression strategies, PGE$_2$/cAMP mimetics, phosphoproteomics using antibodies targeted with high stringency to specific cognate motifs, and amino acid substitutions of ROCK2 to prevent phosphorylation at site S1379. The preponderance of evidence suggests that S1379 is a high stringency PKA site and, in our context, phosphorylated by the PGE$_2$/EP2/cAMP/PKA cassette with no crosstalk from other pathways triggered by PGE$_2$ binding to EP receptors. It is also worth noting that the S1379 site is located in the carboxy-terminal end of ROCK2, which constitutes an autoinhibitory region known to reduce ROCK2 activity [Amano et al., 1999].

The phosphorylation of ROCK2 S1379 site holds interest value because it is the first post-translational modification identified on ROCK2 with a functional cellular process. Although past studies have proven that the cAMP/PKA axis is able to inactivate the RhoA pathway and lead to actin depolymerisation [Dong et al., 1998; Murthy et al., 2003; Goeckeler and Wysolmerski, 2005], our work pinpoints for the first time a precise site of molecular inhibition between PGE$_2$/PKA and ROCK2. This is also a first piece of evidence showing a biological ROCK2 inhibitory signal, a signal so many have examined by comparison to the chemical inhibitor Y27620.

The use of phospho-antibodies and mass spectrophotometry allowed us to generate a large-scale PGE$_2$/GPCR phosphoproteome, providing information regarding signalling networks that essentially control overall cellular responses to the bioactive lipid. One of the more perceptible responses induced by PGE$_2$ was the marked changes in cytoskeletal structure, an effect partly elicited by the inhibition of the RhoA/ROCK2 pathway through specific phosphorylation of S1379 of ROCK2. The biological significance of this may be a regulatory mechanism of functions involving stress fibres and FAs. One such case would be wound repair, which requires the fibroblast formation of stress fibres and FAs by myosin II to generate tension and traction necessary for reparation [Vicente-Manzanares et al., 2009; Bond et al., 2011]. Fibroblasts exhibiting such a phenotype are known to have differentiated into myofibroblasts. The presence of myofibroblasts over a protracted period of time leads to tissue stiffening and fibrosis. Therefore, our experimental model has revealed signalling cues that oppose the formation of stress fibres and FAs that could possibly act as a remedial mode of action against the development of fibrosis. Interestingly, a method of fibrosis treatment involves ROCK2 inhibition by Y26732, which has been shown to reduce fibrosis in animal models [Liu, 2009; Washida et al., 2011]. The first clinical study to report the effects of a Rho-kinase inhibitor was for the treatment in pulmonary hypertension, a condition frequently the outcome of persistent hypoxia associated with pulmonary fibrosis (PF) [Doggrell, 2005; Patel et al., 2007]. In this study, patients with severe pulmonary hypertension were treated with the Rho-kinase inhibitor fasudil and resulted in a significant decrease in pulmonary vascular resistance. In this regard, peptides encompassing the S1379 site with a glutamic acid residue at 1379 (S1379E) will act as a phosphomimetic which could serve as a therapeutic strategy to compete with active WT ROCK2 and control tissue fibrosis potentially with less off-target effects [Jones and Sayers, 2012]. In addition, the antifibrotic parallel between Y26732 and S1379 on ROCK2 provides a strong validation for phosphoproteomic analyses whereby further characterization of the PGE$_2$/GPCR inhibitory signalling pathways may provide potential new targets for therapeutic treatment.

ACKNOWLEDGMENT

REFERENCES

Akhmetshina A, Dees C, Pileckyte M, Szucs G, Spriewald BM, Zwerina J, et al. 2008. Rho-associated kinases are crucial for myofibroblast differentiation and production of extracellular matrix in scleroderma fibroblasts. Arthritis Rheum 58:2553–2564.

Altman R, Asch E, Bloch D, Bole G, Borenstein D, Brandt K, Christy W, Cooke TD. 1986. Classification of osteoarthritis of the knee. Diagnostic and Therapeutic Criteria Committee of the American Rheumatism Association. Arthritis Rheum 29:1039–1049.

Amano M, Ito M, Kimura K, Fukata Y, Chihara K, Nakano T, Matsuura Y, Kaibuchi K. 1996. Phosphorylation and activation of myosin by Rho-associated kinase (Rho-kinase).. J Biol Chem 271:20246–20249.

Amano M, Chibara K, Nakamura N, Kaneto T, Matsuura Y, Kaibuchi K. 1999. The COOH terminus of Rho-kinase negatively regulates rho-kinase activity. J Biol Chem 274:32418–32424.

Ballestrem C, Erez N, Kirchner J, Kam Z, Bershadsky A, Geiger B. 2006. Molecular mapping of tyrosine-phosphorylated proteins in focal adhesions using fluorescence resonance energy transfer. J Cell Sci 119:866–875.

Besser A, Schwarz. 2007. Coupling biochemistry and mechanics in cell adhesion: a model for inhomogeneous stress fiber contraction. New J. Physics 9:425.

Bond J, Ho TQ, Selim MA, Hunter C, Bowers EV, Levinson H.. 2011. Temporal spatial expression and function of non-muscle myosin II isoforms IIA and IIB in scar remodeling. Lab Invest 91(4):499–508.

Butcher DT, Alliston T, Weaver VM. 2009. A tense situation: Forcing tumour progression. Nat Rev Cancer 9:108–122.

Clegg CH, Abrahamsen MS, Degen JL, Morris DR, McKnight. 1992. Cyclic AMP-dependent protein kinase controls basal gene activity and steroidogenesis in Y1 adrenal tumor cells. Biochemistry 31:3720–3726.

Desmoulière A, Darby IA, Gabbiani G. 2003. Normal and pathologic soft tissue remodeling: Role of the myofibroblast, with special emphasis on liver and kidney fibrosis. Lab Invest 83:1689–1707.

Doggrell SA. 2005. Rho-kinase inhibitors show promise in pulmonary hypertension. Expert Opin Invest Drugs 14:1157–1159.

Dong JM, Leung T, Manser E, Lim L. 1998. CAMP-induced morphological changes are counteracted by the activated RhoA small GTPase and the Rho kinase ROKalpha. J Biol Chem 273:22554–22562.

Dreiza CM, Brophy CM, Komalavilas P, Furnish EJ, Joshi L, Pallero MA, et al. 2005. Transducible heat shock protein 20 (HSP20) phosphopeptide alters cytoskeletal dynamics. FASEB J 19:261–263.

Faour WH, Alaaeddine N, Mancini A, He QW, Jovanovic D, Di Battista JA. 2005. Early growth response factor-1 mediates prostaglandin E2-dependent transcriptional suppression of cytokine-induced tumor necrosis factor-alpha gene expression in human macrophages and rheumatoid arthritis-affected synovial fibroblasts. J Biol Chem 280:9536–9546.

Funk CD. 2001. Prostaglandins and leukotrienes: Advances in eicosanoid biology. Science 294:1871–1875.

Goeckeler ZM, Wysolmerski. RB. 2005. Myosin phosphatase and cofilin mediate cAMP/cAMP-dependent protein kinase-induced decline in endothelial cell isometric tension and myosin II regulatory light chain phosphorylation. J Biol Chem 280:33083–33095.

Guarino M, Tosoni A, Nebuloni M. 2009. Direct contribution of epithelium to organ fibrosis: Epithelial-mesenchymal transition. Hum Pathol 40: 1365–1376.

Hinz B. 2007. Formation and function of the myofibroblast during tissue repair. J Invest Dermatol 127:526–537.

Hinz B. 2010. The myofibroblast: Paradigm for a mechanically active cell. J Biomech 43:146–155.

Hinz B, Celetta G, Tomasek JJ, Gabbiani G, Chaponnier C. 2001. Alpha-smooth muscle actin expression upregulates fibroblast contractile activity. Mol Biol Cell 12:2730–2741.

Hochberg MC, Chang RW, Dwosh I, Lindsey S, Pincus T, Wolfe F. 1991. The American College of Rheumatology 1991 revised criteria for the classification of global functional status in rheumatoid arthritis. Arthritis Rheum 35: 498–502.

Horowitz JC, Thannickal VJ. 2006. Epithelial-mesenchymal interactions in pulmonary fibrosis. Semin. Respir. Crit Care Med 27:600–612.

Howe AK. 2004. Regulation of actin-based cell migration by cAMP/PKA. Biochim Biophys Acta 1692:159–174.

Ishizaki T, Maekawa M, Fujisawa K, Okawa K, Iwamatsu A, Fujita A, Watanabe N, Saito Y, Kakizuka A, Morii N, Narumiya, , . 1996. The small GTP-binding protein Rho binds to and activates a 160kDa Ser/Thr protein kinase homologous to myotonic dystrophy kinase. EMBO J 15:1885–1893.

Jones AT, Sayers EJ. 2012. Cell entry of cell penetrating peptides: Tales of tails wagging dogs. J Control Release 161(2):582–591.

Kartberg F, Asp L, Dejgaard SY, Smedh M, Fernandez-Rodriguez J, Nilsson T, Presley JF. 2010. ARFGAP2 and ARFGAP3 are essential for COPI coat assembly on the Golgi membrane of living cells. J Biol Chem 285:36709–36720.

Kolodsick JE, Peters-Golden M, Larios J, Toews GB, Thannickal VJ, Moore BB. 2003. Prostaglandin E2 inhibits fibroblast to myofibroblast transition via E. prostanoid receptor 2 signaling and cyclic adenosine monophosphate elevation. Am J Respir Cell Mol Biol 29:537–544.

Komalavilas P, Penn RB, Flynn CR, Thresher J, Lopes LB, Furnish EJ, et al. 2008. The small heat shock-related protein, HSP20, is a cAMP-dependent protein kinase substrate that is involved in airway smooth muscle relaxation. Am J Physiol Lung Cell Mol Physiol 294:L69–L78.

Liu M, et al. 2009. Therapeutic effect of Y-27632 on chronic allograft nephropathy in rats. J Surg Res 157:117–127.

Moritz A, Li Y, Guo A, Villén J, Wang Y, MacNeill J, Kornhauser J, Sprott K, Zhou J, Possemato A, Min Ren J, Hornbeck P, Cantley LC, Gygi SP, Rush J, Comb MJ. 2010. Akt-RSK-S6 kinase signaling networks activated by oncogenic receptor tyrosine kinases. Sci Signal 3(136):ra64.1–ra64.11.

Murthy KS, Zhou H, Grider JR, Makhlouf GM. 2003. Inhibition of sustained smooth muscle contraction by PKA and PKG preferentially mediated by phosphorylation of RhoA. Am J Physiol Gastrointest Liver Physiol 284: G1006–G1016.

Pasapera AM, Schneider IC, Rericha E, Schlaepfer DD, Waterman CM. 2010. Myosin II activity regulates vinculin recruitment to focal adhesions through FAK-mediated paxillin phosphorylation. J Cell Biol 188:877–890.

Patel NM, Lederer DJ, Borczuk AC, Kawut SM. 2007. Pulmonary hypertension in idiopathic pulmonary fibrosis. Chest 132:998–1006.

Ramachandran C, Patil RV, Combrink K, Sharif NA, Srinivas SP. 2011. 2011. Rho-Rho kinase pathway in the actomyosin contraction and cell-matrix adhesion in immortalized human trabecular meshwork cells. Mol Vis 17:1877–1890.

Sandulache VC, Parekh A, Li-Korotky H, Dohar JE, Hebda PA. 2007. Prostaglandin E2 inhibition of keloid fibroblast migration, contraction, and transforming growth factor (TGF)-beta1-induced collagen synthesis. Wound Repair Regen 15:122–133.

Schneider IC, Hays CK, Waterman, . 2009. Epidermal growth factor-induced contraction regulates paxillin phosphorylation to temporally separate traction generation from de-adhesion. Mol Biol Cell 20:3155–3167.

Song HY1, Kim MY, Kim KH, Lee IH, Shin SH, Lee JS, Kim JH. 2010. Synovial fluid of patients with rheumatoid arthritis induces alpha-smooth muscle actin in human adipose tissue-derived mesenchymal stem cells through a TGF-beta1-dependent mechanism. Exp Mol Med 42(8):565–573.

Steenvoorden, Tolboom TC, van der Pluijm G, Löwik C, Visser CP, DeGroot J, Gittenberger-DeGroot AC, DeRuiter MC, Wisse BJ, Huizinga TW, Toes RE. 2006. Transition of healthy to diseased synovial tissue in rheumatoid arthritis is associated with gain of mesenchymal/fibrotic characteristics. Arthritis Res Ther 8(6):R165.

Stossel TP, Condeelis J, Cooley L, Hartwig JH, Noegel A, Schleicher M, Shapiro SS. 2001. Filamins as integrators of cell mechanics and signalling. Nat Rev Mol Cell Biol 2:138–145.

Strutz F, Okada H, Lo CW, Danoff T, Carone RL, Tomaszewski JE, Neilson EG. 1995. Identification and characterization of a fibroblast marker: FSP1. J Cell Biol 130:393–405.

Thomas PE, Peters-Golden M, White ES, Thannickal VJ, Moore BB. 2007. PGE(2) inhibition of TGF-beta1-induced myofibroblast differentiation is Smad-independent but involves cell shape and adhesion-dependent signalling. Am J Physiol Lung Cell Mol Physiol 293:L417–L428.

Tomasek JJ, Gabbiani G, Hinz B, Chaponnier C, Brown RA. 2002. Myofibroblasts and mechano-regulation of connective tissue remodelling. Nat Rev Mol Cell Biol 3:349–363.

Tomasek JJ, Vaughan MB, Kropp BP, Gabbiani G, Martin MD, Haaksma CJ, Hinz B. 2006. Contraction of myofibroblasts in granulation tissue is dependent on Rho/Rho kinase/myosin light chain phosphatase activity. Wound Repair Regen . 14:313–320.

Turner CE. 2000. Paxillin and focal adhesion signalling. Nat Cell Biol 2:E231–E236.

Vicente-Manzanares M, Ma X, Adelstein RS, Horwitz AR. 2009. Non-muscle myosin II takes centre stage in cell adhesion and migration. Nat Rev Mol Cell Biol 10:778–790.

Washida N, Wakino S, Tonozuka Y, Homma K, Tokuyama H, Hara Y, Haseqawa K, et al. 2011. Rho-kinase inhibition ameliorates peritoneal fibrosis and angiogenesis in a rat model of peritoneal sclerosis. Nephrol Dial Transplant 26:2770–2779.

Woo MS, Ohta Y, Rabinovitz I, Stossel TP, Blenis J. 2004. Ribosomal S6 kinase (RSK) regulates phosphorylation of filamin A on an important regulatory site. Mol Cell Biol 24:3025–3035.

Wozniak MA, Modzelewska K, Kwong L, Keely PJ. 2004. Focal adhesion regulation of cell behavior. Biochim Biophys Acta 1692:103–119.

Zhai B, Yang H, Mancini A, He QW, Antoniou J, Di Battista. 2010. Leukotriene B(4) BLT receptor signaling regulates the level and stability of cyclooxygenase-2 (COX-2) mRNA through restricted activation of Ras/Raf/ERK/p42 AUF1 pathway. J Biol Chem 285:23568–23580.

Zimmermann T, Kunisch E, Pfeiffer R, Hirth A, Hans-Detlev Stahl H-D, Sack U, Laube A, Liesaus E, Roth A, Palombo-Kinne E, Emmrich F. 2001. Isolation and characterization of rheumatoid arthritis synovial fibroblasts from primary culture−Primary culture cells markedly differ from fourth-passage cells. Arthritis Res 3:72–76.